Production of Orbitally Excited Charm Mesons in Semileptonic B Decays

The ALEPH Collaboration

Abstract

A sample of 3.6 million hadronic Z decays recorded between 1991 and 1995 with the ALEPH detector at LEP is used to investigate semileptonic decays of B mesons into final states involving orbitally excited charm mesons. Topological vertex criteria are used to search for decays involving narrow D^{**} states as well as wide D^{**} resonances and non-resonant $D^{(*)}\pi$ final states. The sum of the branching ratios for these processes is measured to be

$$\mathrm{Br}(\overline{\mathrm{B}} \to \mathrm{D}\pi\ell^-\overline{\nu}) + \mathrm{Br}(\overline{\mathrm{B}} \to \mathrm{D}^*\pi\ell^-\overline{\nu}) = (2.26 \pm 0.29(\mathrm{stat}) \pm 0.33(\mathrm{syst}))\%,$$

which accounts for a significant fraction of the deficit between inclusive measurements and the sum of exclusive semileptonic B decay modes.

The ALEPH Collaboration

D. Buskulic, I. De Bonis, D. Decamp, P. Ghez, C. Goy, J.-P. Lees, A. Lucotte, M.-N. Minard, J.-Y. Nief,
P. Odier, B. Pietrzyk

Laboratoire de Physique des Particules (LAPP), IN[2]P[3]-CNRS, 74019 Annecy-le-Vieux Cedex, France

M.P. Casado, M. Chmeissani, J.M. Crespo, M. Delfino, I. Efthymiopoulos,[1] E. Fernandez, M. Fernandez-Bosman, Ll. Garrido,[15] A. Juste, M. Martinez, S. Orteu, C. Padilla, I.C. Park, A. Pascual, J.A. Perlas,
I. Riu, F. Sanchez, F. Teubert

*Institut de Fisica d'Altes Energies, Universitat Autonoma de Barcelona, 08193 Bellaterra (Barcelona),
Spain[7]*

A. Colaleo, D. Creanza, M. de Palma, G. Gelao, M. Girone, G. Iaselli, G. Maggi,[3] M. Maggi, N. Marinelli,
S. Nuzzo, A. Ranieri, G. Raso, F. Ruggieri, G. Selvaggi, L. Silvestris, P. Tempesta, G. Zito

Dipartimento di Fisica, INFN Sezione di Bari, 70126 Bari, Italy

X. Huang, J. Lin, Q. Ouyang, T. Wang, Y. Xie, R. Xu, S. Xue, J. Zhang, L. Zhang, W. Zhao

Institute of High-Energy Physics, Academia Sinica, Beijing, The People's Republic of China[8]

R. Alemany, A.O. Bazarko, G. Bonvicini,[23] P. Bright-Thomas, M. Cattaneo, P. Comas, P. Coyle,
H. Drevermann, R.W. Forty, M. Frank, R. Hagelberg, J. Harvey, P. Janot, B. Jost, E. Kneringer,
J. Knobloch, I. Lehraus, G. Lutters, E.B. Martin, P. Mato, A. Minten, R. Miquel, Ll.M. Mir,[2] L. Moneta,
T. Oest,[20] A. Pacheco, J.-F. Pusztaszeri, F. Ranjard, P. Rensing,[12] G. Rizzo, L. Rolandi, D. Schlatter,
M. Schmelling,[24] M. Schmitt, O. Schneider, W. Tejessy, I.R. Tomalin, A. Venturi, H. Wachsmuth,
A. Wagner

European Laboratory for Particle Physics (CERN), 1211 Geneva 23, Switzerland

Z. Ajaltouni, A. Barrès, C. Boyer, A. Falvard, P. Gay, C . Guicheney, P. Henrard, J. Jousset, B. Michel,
S. Monteil, J-C. Montret, D. Pallin, P. Perret, F. Podlyski, J. Proriol, P. Rosnet, J.-M. Rossignol

*Laboratoire de Physique Corpusculaire, Université Blaise Pascal, IN[2]P[3]-CNRS, Clermont-Ferrand,
63177 Aubière, France*

T. Fearnley, J.B. Hansen, J.D. Hansen, J.R. Hansen, P.H. Hansen, B.S. Nilsson, B. Rensch, A. Wäänänen

Niels Bohr Institute, 2100 Copenhagen, Denmark[9]

A. Kyriakis, C. Markou, E. Simopoulou, I. Siotis, A. Vayaki, K. Zachariadou

Nuclear Research Center Demokritos (NRCD), Athens, Greece

A. Blondel, G. Bonneaud, J.C. Brient, P. Bourdon, A. Rougé, M. Rumpf, A. Valassi,[6] M. Verderi,
H. Videau[21]

*Laboratoire de Physique Nucléaire et des Hautes Energies, Ecole Polytechnique, IN[2]P[3]-CNRS, 91128
Palaiseau Cedex, France*

D.J. Candlin, M.I. Parsons

Department of Physics, University of Edinburgh, Edinburgh EH9 3JZ, United Kingdom[10]

E. Focardi,[21] G. Parrini

Dipartimento di Fisica, Università di Firenze, INFN Sezione di Firenze, 50125 Firenze, Italy

M. Corden, C. Georgiopoulos, D.E. Jaffe

*Supercomputer Computations Research Institute, Florida State University, Tallahassee, FL 32306-
4052, USA [13,14]*

A. Antonelli, G. Bencivenni, G. Bologna,[4] F. Bossi, P. Campana, G. Capon, D. Casper, V. Chiarella,
G. Felici, P. Laurelli, G. Mannocchi,[5] F. Murtas, G.P. Murtas, L. Passalacqua, M. Pepe-Altarelli

Laboratori Nazionali dell'INFN (LNF-INFN), 00044 Frascati, Italy

L. Curtis, S.J. Dorris, A.W. Halley, I.G. Knowles, J.G. Lynch, V. O'Shea, C. Raine, P. Reeves, J.M. Scarr,

K. Smith, P. Teixeira-Dias, A.S. Thompson, F. Thomson, S. Thorn, R.M. Turnbull

 Department of Physics and Astronomy, University of Glasgow, Glasgow G12 8QQ,United Kingdom[10]

U. Becker, C. Geweniger, G. Graefe, P. Hanke, G. Hansper, V. Hepp, E.E. Kluge, A. Putzer, M. Schmidt, J. Sommer, H. Stenzel, K. Tittel, S. Werner, M. Wunsch

 Institut für Hochenergiephysik, Universität Heidelberg, 69120 Heidelberg, Fed. Rep. of Germany[16]

D. Abbaneo, R. Beuselinck, D.M. Binnie, W. Cameron, P.J. Dornan, A. Moutoussi, J. Nash, J.K. Sedgbeer, A.M. Stacey, M.D. Williams

 Department of Physics, Imperial College, London SW7 2BZ, United Kingdom[10]

G. Dissertori, P. Girtler, D. Kuhn, G. Rudolph

 Institut für Experimentalphysik, Universität Innsbruck, 6020 Innsbruck, Austria[18]

A.P. Betteridge, C.K. Bowdery, P. Colrain, G. Crawford, A.J. Finch, F. Foster, G. Hughes, T. Sloan, M.I. Williams

 Department of Physics, University of Lancaster, Lancaster LA1 4YB, United Kingdom[10]

A. Galla, I. Giehl, A.M. Greene, K. Jakobs, K. Kleinknecht, G. Quast, B. Renk, E. Rohne, H.-G. Sander, P. van Gemmeren C. Zeitnitz

 Institut für Physik, Universität Mainz, 55099 Mainz, Fed. Rep. of Germany[16]

J.J. Aubert,[21] A.M. Bencheikh, C. Benchouk, A. Bonissent, G. Bujosa, D. Calvet, J. Carr, C. Diaconu, F. Etienne, N. Konstantinidis, P. Payre, D. Rousseau, M. Talby, A. Sadouki, M. Thulasidas, K. Trabelsi

 Centre de Physique des Particules, Faculté des Sciences de Luminy, IN^2P^3-CNRS, 13288 Marseille, France

M. Aleppo, F. Ragusa[21]

 Dipartimento di Fisica, Università di Milano e INFN Sezione di Milano, 20133 Milano, Italy

C. Bauer, R. Berlich, W. Blum, V. Büscher, H. Dietl, F. Dydak,[21] G. Ganis, C. Gotzhein, H. Kroha, G. Lütjens, G. Lutz, W. Männer, H.-G. Moser, R. Richter, A. Rosado-Schlosser, S. Schael, R. Settles, H. Seywerd, R. St. Denis, H. Stenzel, W. Wiedenmann, G. Wolf

 Max-Planck-Institut für Physik, Werner-Heisenberg-Institut, 80805 München, Fed. Rep. of Germany[16]

J. Boucrot, O. Callot, Y. Choi,[26] A. Cordier, M. Davier, L. Duflot, J.-F. Grivaz, Ph. Heusse, A. Höcker, A. Jacholkowska, M. Jacquet, D.W. Kim,[19] F. Le Diberder, J. Lefrançois, A.-M. Lutz, I. Nikolic, H.J. Park,[19] M.-H. Schune, S. Simion, J.-J. Veillet, I. Videau, D. Zerwas

 Laboratoire de l'Accélérateur Linéaire, Université de Paris-Sud, IN^2P^3-CNRS, 91405 Orsay Cedex, France

P. Azzurri, G. Bagliesi, G. Batignani, S. Bettarini, C. Bozzi, G. Calderini, M. Carpinelli, M.A. Ciocci, V. Ciulli, R. Dell'Orso, R. Fantechi, I. Ferrante, L. Foà,[1] F. Forti, A. Giassi, M.A. Giorgi, A. Gregorio, F. Ligabue, A. Lusiani, P.S. Marrocchesi, A. Messineo, F. Palla, G. Sanguinetti, A. Sciabà, P. Spagnolo, J. Steinberger, R. Tenchini, G. Tonelli,[25] C. Vannini, P.G. Verdini, J. Walsh

 Dipartimento di Fisica dell'Università, INFN Sezione di Pisa, e Scuola Normale Superiore, 56010 Pisa, Italy

G.A. Blair, L.M. Bryant, F. Cerutti, J.T. Chambers, Y. Gao, M.G. Green, T. Medcalf, P. Perrodo, J.A. Strong, J.H. von Wimmersperg-Toeller

 Department of Physics, Royal Holloway & Bedford New College, University of London, Surrey TW20 OEX, United Kingdom[10]

D.R. Botterill, R.W. Clifft, T.R. Edgecock, S. Haywood, P. Maley, P.R. Norton, J.C. Thompson, A.E. Wright

 Particle Physics Dept., Rutherford Appleton Laboratory, Chilton, Didcot, Oxon OX11 OQX, United Kingdom[10]

B. Bloch-Devaux, P. Colas, S. Emery, W. Kozanecki, E. Lançon, M.C. Lemaire, E. Locci, B. Marx, P. Perez, J. Rander, J.-F. Renardy, A. Roussarie, J.-P. Schuller, J. Schwindling, A. Trabelsi, B. Vallage

 CEA, DAPNIA/Service de Physique des Particules, CE-Saclay, 91191 Gif-sur-Yvette Cedex, France[17]

S.N. Black, J.H. Dann, R.P. Johnson, H.Y. Kim, A.M. Litke, M.A. McNeil, G. Taylor

Institute for Particle Physics, University of California at Santa Cruz, Santa Cruz, CA 95064, USA[22]

C.N. Booth, R. Boswell, C.A.J. Brew, S. Cartwright, F. Combley, A. Koksal, M. Letho, W.M. Newton, J. Reeve, L.F. Thompson

Department of Physics, University of Sheffield, Sheffield S3 7RH, United Kingdom[10]

A. Böhrer, S. Brandt, G. Cowan, C. Grupen, J. Minguet-Rodriguez, F. Rivera, P. Saraiva, L. Smolik, F. Stephan,

Fachbereich Physik, Universität Siegen, 57068 Siegen, Fed. Rep. of Germany[16]

M. Apollonio, L. Bosisio, R. Della Marina, G. Giannini, B. Gobbo, G. Musolino

Dipartimento di Fisica, Università di Trieste e INFN Sezione di Trieste, 34127 Trieste, Italy

J. Rothberg, S. Wasserbaech

Experimental Elementary Particle Physics, University of Washington, WA 98195 Seattle, U.S.A.

S.R. Armstrong, P. Elmer, Z. Feng,[27] D.P.S. Ferguson, Y.S. Gao,[28] S. González, J. Grahl, T.C. Greening, O.J. Hayes, H. Hu, P.A. McNamara III, J.M. Nachtman, W. Orejudos, Y.B. Pan, Y. Saadi, I.J. Scott, A.M. Walsh,[29] Sau Lan Wu, X. Wu, J.M. Yamartino, M. Zheng, G. Zobernig

Department of Physics, University of Wisconsin, Madison, WI 53706, USA[11]

1 Introduction

A sizeable fraction of semileptonic B decays is not accounted for by the measured branching ratios for $\overline{\mathrm{B}} \to \mathrm{D}\ell^-\overline{\nu}$ and $\overline{\mathrm{B}} \to \mathrm{D}^*\ell^-\overline{\nu}$, contrary to initial theoretical expectations [1]. It is therefore interesting to search for other exclusive semileptonic decays such as direct four-body decays, $\overline{\mathrm{B}} \to \mathrm{D}^{(*)}\pi\ell^-\overline{\nu}$, or $\overline{\mathrm{B}} \to \mathrm{D}^{**}\ell^-\overline{\nu}$, where D^{**} represents an orbitally excited (P-wave) charm meson.

Heavy Quark Effective Theory (HQET) predicts the existence and properties of four neutral and four charged D^{**} mesons [2]. In the limit of infinite heavy–quark mass, the total angular momentum of the light quark degrees of freedom J_{lq} is a good quantum number and can be used to classify the physical states into two doublets of $\mathrm{J}_{\mathrm{lq}} = 1/2$ and $3/2$. The $\mathrm{J}_{\mathrm{lq}} = 1/2$ states are expected to be wide, since they undergo S-wave decays, while the $\mathrm{J}_{\mathrm{lq}} = 3/2$ are expected to be narrow since only D-wave decays are allowed. Evidence has been established for both the neutral [3] and charged [4] states of the narrow $\mathrm{J}_{\mathrm{lq}} = 3/2$ states through their two-body decays. The wide $\mathrm{J}_{\mathrm{lq}} = 1/2$ states are experimentally unobserved and are difficult to separate from four-body decays with the present ALEPH data sample. Table 1 gives the properties of the D^{**} states.

	J^{P}	J_{lq}	Neutral states		Charged states		Decay Modes
			Mass (MeV/c^2)	Width (MeV/c^2)	Mass (MeV/c^2)	Width (MeV/c^2)	
D_1^*	1^+	$1/2$	~ 2420	$\gtrsim 250$	~ 2420	$\gtrsim 250$	$\mathrm{D}^*\pi$
D_0^*	0^+	$1/2$	~ 2360	$\gtrsim 170$	~ 2360	$\gtrsim 170$	$\mathrm{D}\pi$
D_1	1^+	$3/2$	2422 ± 2	19 ± 4	2427 ± 5	28 ± 8	$\mathrm{D}^*\pi$
D_2^*	2^+	$3/2$	2459 ± 2	23 ± 5	2459 ± 4	25 ± 8	$\mathrm{D}\pi, \mathrm{D}^*\pi$

Table 1: The quantum numbers, masses, widths, and allowed strong decays into $\mathrm{D}\pi$ and $\mathrm{D}^*\pi$ of charm mesons with orbital excitations, in the infinite heavy–quark mass limit. Masses and widths of the narrow $\mathrm{J}_{\mathrm{lq}} = 3/2$ states are experimentally determined [5]; the values for the wide $\mathrm{J}_{\mathrm{lq}} = 1/2$ states are theoretical estimates [6].

This paper presents a measurement of decay modes involving the narrow D_1 and D_2^* states ($\overline{\mathrm{B}} \to \mathrm{D}_1\ell^-\overline{\nu}X$ and $\overline{\mathrm{B}} \to \mathrm{D}_2^*\ell^-\overline{\nu}X$)[1] . In the following sections, this will be referred to as the *narrow–resonance* analysis. A measurement of the sum of resonant (narrow and wide) and four–body decay rates is also performed relying only on the topological properties of signal events; this will be referred to as the *topological* analysis. The experimental method is based on the detached vertex topology of B decays at the Z resonance, and, for the narrow–resonance analysis, on the presence of narrow resonant structures in invariant mass distributions. Both analyses rely heavily on the excellent momentum and position resolution of the ALEPH tracking system. Three different final state samples are used: $\mathrm{D}^0\pi^+\ell^-$, $\mathrm{D}^{*+}\pi^-\ell^-$ and $\mathrm{D}^+\pi^-\ell^-$.

The results obtained in this paper for narrow states and topological decays via $\mathrm{D}^{*+}\pi^-\ell^-$ supersede a published ALEPH analysis [7]. Evidence for narrow D^{**} states in semileptonic B decays has been previously reported by ARGUS [8], OPAL [9], and CLEO [10]. DELPHI has reported evidence for topological decays via $\mathrm{D}^{*+}\pi^-\ell^-$ [11].

---

[1] In this paper, charge conjugate reactions are always implied.

The layout of this paper is as follows. The relevant aspects of the ALEPH detector and its performance are discussed in Section 2. Event selection criteria are described in Section 3. Results for the study of decays via narrow D^{**} states and topological $D^{(*)}\pi$ final states are presented in sections 4 and 5. The results are summarized and discussed in Section 6. Conclusions are presented in Section 7.

2 The ALEPH Detector

The ALEPH detector and its performance are described in detail elsewhere [12, 13]. This section presents only a brief description of the parts of the apparatus most relevant to this analysis.

Charged particles are reconstructed by means of three concentric tracking devices surrounded by a superconducting coil which provides an axial magnetic field of 1.5 T. The vertex detector (VDET) [14] consists of silicon microstrip detectors with strip readout in two orthogonal directions. The detectors surround the beam pipe and are arranged in two cylindrical layers at average radii of 6.5 and 11.3 cm. The solid angle coverage is 85% for the inner layer and 69% for the outer layer. The point resolution for tracks at normal incidence is 12 μm in both the $r\phi$ and z projections. A cylindrical drift chamber (ITC) with up to eight measurements in the $r\phi$ projection surrounds the VDET. Outside the ITC, the time projection chamber (TPC) provides up to 21 space points for $|\cos\theta| < 0.79$, and a decreasing number of points for smaller angles, with four at $|\cos\theta| = 0.96$. The transverse momentum resolution for the combined tracking system is $\Delta p_t/p_t = 0.0006 \times p_t \oplus 0.005$ (p_t in GeV/c). The impact parameter resolution of a track of momentum p, with hits in both VDET layers, is 25 μm + 95 μm/p (p in GeV/c).

The TPC is also used for particle identification by measurement of the ionization energy loss associated with each charged track. Up to 338 dE/dx measurements per track can be provided, with a measured resolution of 4.5% for Bhabha electrons with at least 330 ionization samples. For charged particles with momenta above 2 GeV/c, the mean dE/dx gives $\approx 2\,\sigma$ separation between kaons and pions.

In the following sections, particle identification using energy loss is specified in terms of the dE/dx estimator defined as $R_x = (I_{\mathrm{meas}} - I_x)/\sigma_x$, where I_{meas} is the measured energy loss, I_x the expected energy loss under the hypothesis that the candidate x is a π or a K and σ_x is the expected resolution on I_x. Studies on simulated events have shown that the criterion $R_{\mathrm{K}} + R_\pi < 1$ is more effective in selecting kaons and rejecting pions than a simple one–dimensional requirement on R_{K} or R_π. The dE/dx is considered available if more than 50 samples are present. This occurs for 82% of the tracks in hadronic decays and is well reproduced in Monte Carlo simulations.

A lead/proportional chamber sampling electromagnetic calorimeter (ECAL) surrounds the TPC and provides an energy resolution of $\Delta E/E = 0.165/\sqrt{E} + 0.003$ (E in GeV). The ECAL is arranged in 15 mrad $\times$ 15 mrad projective towers and is read out in three sections in depth.

Outside the coil, the iron return yoke is instrumented with streamer tubes to form the hadron calorimeter (HCAL) of over 7 interaction lengths thickness. The HCAL is surrounded by two additional layers of streamer tubes used for muon identification.

Lepton identification in ALEPH is described in detail in reference [15]. Electrons are

identified by comparing the energy deposit in the ECAL with the momentum measured in the tracking system, the shape and depth of the ECAL energy deposit and the specific ionization measurement. Muon candidates are required to have a hit pattern characteristic of a penetrating particle in the HCAL and at least two associated hits in the muon chambers.

The results presented in this paper are based on 3.6×10^6 hadronic Z decays collected with the ALEPH detector at LEP from 1991 to 1995.

3   Event Selection

This analysis searches for semileptonic B decays with a $D^{(*)}\pi$ pair in the final state. These include non-resonant decays $\overline{B} \rightarrow D^{(*)}\pi\ell^-\overline{\nu}$ as well as the following decays through charged or neutral D^{**} states.

$$\overline{B} \longrightarrow D^{**+}\ell^-\overline{\nu}X$$
$$\hookrightarrow D^0\ \pi^+_{**}$$
$$\hookrightarrow D^{*0}\ \pi^+_{**}$$
$$\hookrightarrow D^0\pi^0/\gamma$$

$$\overline{B} \longrightarrow D^{**0}\ell^-\overline{\nu}X$$
$$\hookrightarrow D^+\pi^-_{**}$$
$$\hookrightarrow D^{*+}\pi^-_{**}$$
$$\hookrightarrow D^0\pi^+$$
$$\hookrightarrow D^+\pi^0/\gamma$$

Here π_{**} denotes the charged pion from D^{**} decay. The symbol π_{**} is used throughout this paper also to denote pions in non-resonant $D^{(*)}\pi$ final states since the relevant topologies and selection criteria are similar. The neutral pion or photon from D^{*0} or D^{*+} decays is not reconstructed.

Signal processes for both narrow–resonance and topological cases have the same vertex topology. For example, Fig. 1 illustrates the topology for semileptonic B decay into a D^{**+} which decays into $D^0\ \pi^+_{**}$. A semileptonic B decay to a four-body $D^0\pi^+\ell^-\overline{\nu}$ state would have the same topology.

Starting from inclusive $D^0\ell^-$, $D^{*+}\ell^-$, and $D^+\ell^-$ samples, $D^{(*)}$ candidates are paired with π_{**} candidates. The main background to the signal processes is due to semileptonic B decays into a D^0, D^{*+}, or D^+ where the π_{**} is actually a fragmentation track mistakenly associated to the B vertex. This is referred to as *fragmentation background*. Another source of background is due to fake combinations when reconstructing the D^0, D^{*+}, or D^+, which is referred to as *combinatorial background*.

3.1   Charm-Lepton Selection

Selection criteria for obtaining inclusive $D^0\ell^-$, $D^{*+}\ell^-$, and $D^+\ell^-$ samples are summarized below. Most of the requirements are common to the analysis of narrow–resonance and topological decays. Hadronic events containing a high momentum lepton and a D^0, D^{*+}, or D^+ meson, fully reconstructed in a cone of $45°$ around the lepton, are selected. Electron candidates are required to have a momentum greater than 2 GeV/c; muon candidates are required to have a momentum greater than 3 GeV/c.
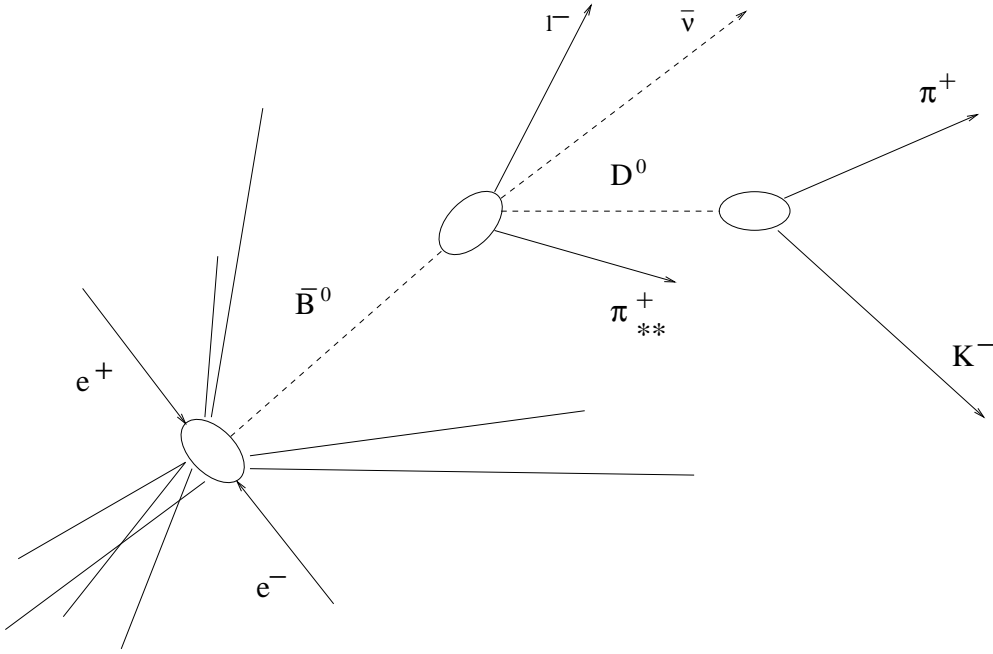
Figure 1: Vertex topology for a semileptonic B decay in D^{**+}, which decays into $D^0\pi^+_{**}$, as described in the text.

$D^0\ell^-$ Selection: The D^0 is reconstructed in four decay channels:
$D^0 \to K^-\pi^+$, $D^0 \to K^-\pi^+\pi^-\pi^+$, $D^0 \to K^0_S\pi^+\pi^-$, and $D^0 \to K^-\pi^+\pi^0$.

The momentum of the D^0 is required to be greater than 5 GeV/c for the $K^-\pi^+$ and $K^-\pi^+\pi^-\pi^+$ decays, 10 GeV/c for the $K^-\pi^+\pi^0$ decay, and 7 GeV/c for the $K^0_S\pi^+\pi^-$ decay. For the $K^-\pi^+\pi^-\pi^+$ and $K^-\pi^+\pi^0$ modes, the specific ionization measurement of the K candidate, when available, must satisfy $R_K + R_\pi < 1$, with R_x defined in Section 2; the combination is rejected if the kaon candidate has a momentum lower than 1.5 GeV/c. The combinatorial background is further reduced in the $D^0 \to K^-\pi^+\pi^-\pi^+$ decay by means of the track probability to originate from the primary vertex. This quantity, defined and described in detail in [16], is required to be less than 5% for at least three of the D^0 decay tracks; moreover, such tracks must be downstream of the primary vertex. Neutral pions in the $D^0 \to K^-\pi^+\pi^0$ decay mode are identified by fitting pairs of ECAL energy deposits using the constraint that the mass of the pair is consistent with the π^0 mass. The D^0 decays into $K^-\pi^+\pi^0$ mode are reconstructed selecting $\pi\pi$ and $K\pi$ combinations with masses within ± 2 half-widths of the ρ, K^{*-} or $\overline{K}^{*0}$ resonances. In $D^0 \to K^0_S\pi^+\pi^-$, the same technique is applied to the K^{*-} resonance. K^0_S candidates are rejected if the measured mass is more than 2σ ($\pm 10 \,\mathrm{MeV}/c^2$) from the nominal K^0_S mass. Pions from the K^0_S decay are required to be inconsistent with tracks originating from the interaction point.

The mass of the D^0 candidates must lie within $\pm 2\sigma$ of the nominal D^0 mass, where σ is the standard deviation of the fit to the D^0 mass distribution. To eliminate contamination from D^{*+} decays, other charged tracks (denoted as "π") are paired with the reconstructed D^0; the event is rejected if any combination has a mass difference $\mid m(D^{0``}\pi") - m(D^0)\mid$ less than 5 MeV/c^2 (the resolution on this quantity is $\sigma \sim 0.7 \,\mathrm{MeV}/c^2$) from the nominal value of 145.5 MeV/c^2.

Reconstructed D^0 mesons and leptons are fitted to a common B vertex. Both the D^0 and $D^0\ell^-$ vertices are required to have a vertex χ^2 probability greater than 1%.

4

Defining the B (D) vertex *significance* $\mathcal{S}_{B(D)}$ as the ratio of the distance of the $D^{(*)}\ell^-$ (D) vertex from the primary $(D^{(*)}\ell^-)$ vertex over its uncertainty $\sigma_{B(D)}$, $D^0\ell^-$ combinations are rejected if $\mathcal{S}_B < 3$ or $\sigma_B > 500$ μm. The $D^0\ell^-$ vertex is required to be upstream of the D^0 vertex $(\mathcal{S}_D > 0)$. The invariant mass of the $D^0\ell^-$ system is required to be between 2.7 and 5 GeV/c^2 for the narrow–resonance analysis and between 3.0 and 5 GeV/c^2 for the topological analysis.

$D^{*+}\ell^-$ Selection: The D^{*+} is reconstructed in the channel $D^{*+} \to D^0\pi^+$. The D^0 is reconstructed in the same four decay modes used in the $D^0\ell^-$ selection. However, the presence of a narrow D^{*+} resonance permits a strong suppression of the combinatorial background. Therefore some kinematic and topological cuts for this sample can be loosened with respect to the $D^0\ell^-$ sample. Namely, the D^0 momentum cut is lowered to $5\,\text{GeV}/c$ and $8\,\text{GeV}/c$ for the $K_S^0\,\pi^+\pi^-$ and $K^-\pi^+\pi^0$ modes respectively; for the $K^-\pi^+\pi^-\pi^+$ mode, at least two tracks must have momentum greater than $1\,\text{GeV}/c$. The mass difference $m(D^0\pi^+) - m(D^0)$ is required to be within two standard deviations of 145.5 MeV/c^2 and the B vertex must have a significance $\mathcal{S}_B > 2$. The invariant mass of the $D^{*+}\ell^-$ system is required to be between 2.7 and 4.5 GeV/c^2 for the narrow–resonance analysis and between 3.0 and 4.5 GeV/c^2 for the topological analysis.

$D^+\ell^-$ Selection: The D^+ is reconstructed in the decay channel $D^+ \to K^-\pi^+\pi^+$. The momentum of the K^- is required to be greater than 2 GeV/c. The same ionization measurement criteria as above are required for the K^- candidate. The momentum of each π^+ from the D^+ is required to be greater than 1.5 GeV/c. A cut is also made on the track probability to originate from the interaction point, as described above, in order to reject combinatorial background; the probabilities for the three D^+ decay tracks are required to be below 5% and all the tracks have to be downstream of the primary vertex. The mass of the D^+ candidate must lie within $\pm 2\sigma$ of the nominal D^+ mass, where σ is the standard deviation of the fit to the D^+ mass distribution. Reconstructed D^+ mesons and leptons are fitted to a common vertex; both D^+ and the $D^+\ell^-$ vertices must have a χ^2 probability greater than 1%, decay length significances $\mathcal{S}_B > 2$, $\mathcal{S}_D > 0$ and $\sigma_B < 500\mu$m. The invariant mass of the $D^+\ell^-$ system is required to be between 2.7 and 4.5 GeV/c^2 for the narrow–resonance analysis and between 3.0 and 4.5 for the topological analysis.

The mass resolution and the signal and combinatorial background rates for the three $D^{(*)}\ell^-$ samples are summarized in Table 2.

3.2 π_{**} Selection

True π_{**} have a harder momentum spectrum than fragmentation tracks. For this reason, π_{**} candidates are rejected if their momentum is less than 1 GeV/c. This momentum cut also reduces uncertainties due to multiple scattering.

A π_{**} candidate is required to have an unambiguous topology to eliminate contamination from fragmentation pions. Thus, defining the *impact parameter significance* $\mathcal{S}_{PV}$ as the ratio of the impact parameter of the π_{**} with respect to the primary vertex over its uncertainty σ_{PV}, only candidates with $\mathcal{S}_{PV} > 1$ for the neutral $D^{*+}\pi_{**}^-$ and $D^+\pi_{**}^-$ modes and $\mathcal{S}_{PV} > 2$ for the charged $D^0\pi_{**}^+$ mode are retained in the narrow–resonance analysis. For the topological analysis, these cuts are tightened to 2.5 and 3 respectively.

Channel	mass resolution (MeV/c^2)	$D\ell^-$ signal	Combinatorial background	$D^*\ell^-$ signal	Combinatorial background
$D^0, D^{*+}\ell^-$ samples					
$D^0 \to K^-\pi^+$	10	847±37	270±14	386±20	8±2
$D^0 \to K^-\pi^+\pi^-\pi^+$	7	517±29	169±8	520±26	86±7
$D^0 \to K^0_S\pi^+\pi^-$	8	222±17	40±5	107±12	8±2
$D^0 \to K^-\pi^+\pi^0$	26	453±22	106±10	296±21	48±5
$D^+\ell^-$ sample					
$D^+ \to K^-\pi^+\pi^+$	9	268±19	48±4		

Table 2: Mass resolutions and fitted number of signal and combinatorial background events within a $\pm 2\sigma$ window around the fitted $D^{(*)}$ mass for the $D^0\ell^-$, $D^{*+}\ell^-$, and $D^+\ell^-$ samples.
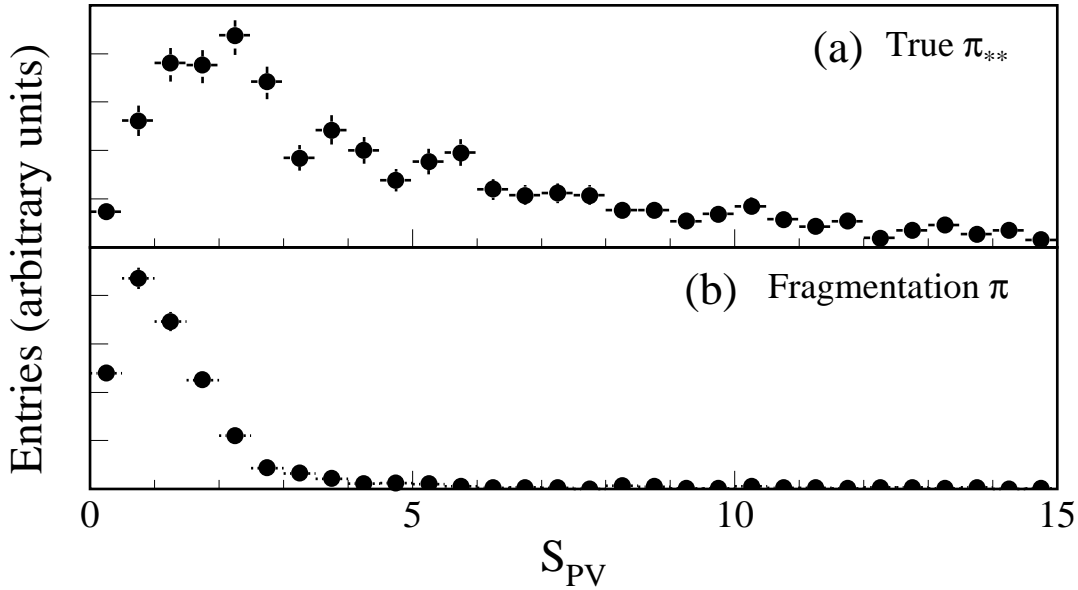

Figure 2: Impact parameter significance with respect to the primary vertex for true π_{**} (a) and fragmentation tracks (b) in the $D^0\pi^+_{**}$ mode.

As an illustration, Fig. 2 shows the $\mathcal{S}_{PV}$ distribution for true π_{**} and fragmentation tracks from Monte Carlo simulations of the $D^0\pi^+_{**}$ mode.

The distribution of the impact parameter significance $\mathcal{S}_{SV}$ with respect to the secondary vertex $D^{(*)}\ell^-$, defined in a similar way, is used to construct a cumulative probability function which gives the probability $\mathcal{P}$ that the π_{**} originates from the $D^{(*)}\ell^-$ vertex. This procedure is described in detail in [7]. Only π_{**} candidates with $\sigma_{SV} < 250\mu m$ are accepted for the narrow–resonance analysis; this cut is tightened to $\sigma_{SV} < 150\mu m$ for the topological analysis. Figure 3 shows the $\mathcal{P}$ distribution for simulated signal events and fragmentation background events in the $D^0\pi^+_{**}$ mode. The $\mathcal{P}$ distribution for the signal is expected to be flat by construction, while it peaks at zero for the background.

For the narrow–resonance analysis the π_{**} candidates are accepted if they have $\mathcal{P} > 0.1$, which eliminates 80% of the fragmentation background. This cut is tightened to $\mathcal{P} > 0.2$ for the topological analysis. If more than one $D\ell\pi_{**}$ combination per event is found, the π_{**} with the greatest probability $\mathcal{P}$ is chosen in the narrow–resonance analysis; for the topological case, the π_{**} with the highest momentum is selected. There are multiple combinations for only 3%-5% of the events, depending on the channel. The reconstruction
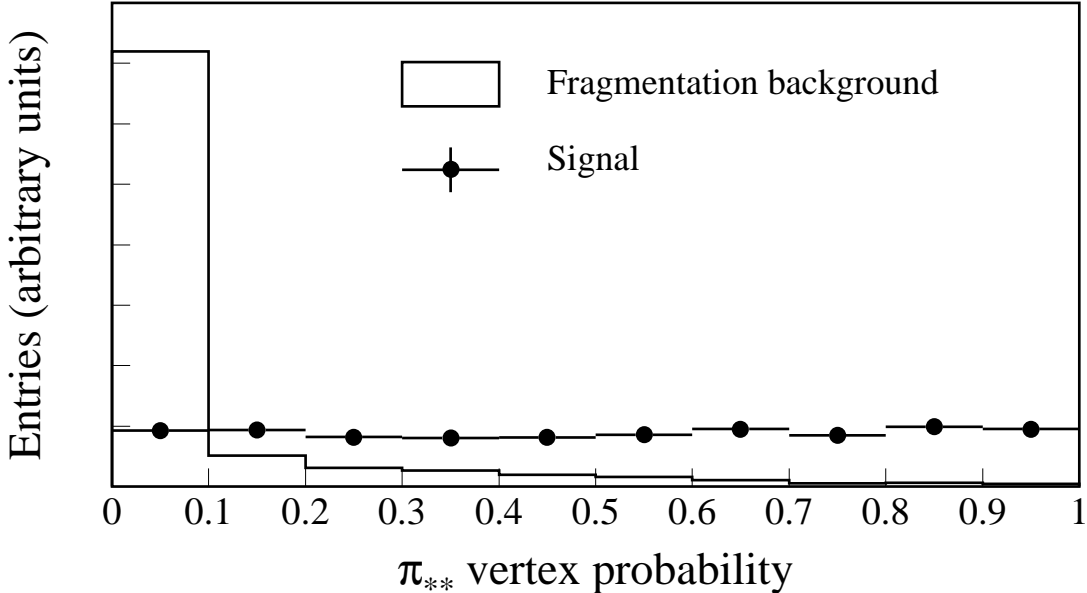

Figure 3: Distributions of the probability $\mathcal{P}$ for simulated signal (dots) and fragmentation background (histogram) events in the $D^0\pi_{**}^+$ mode. Both contributions have been normalized to the same area.

efficiencies for signal processes for the narrow–resonance analysis in the $D^0\pi_{**}^+\ell^-$, $D^{*+}\pi_{**}^-\ell^-$ and $D^+\pi_{**}^-\ell^-$ samples are summarized in Table 3. The overall efficiencies, including $D^{(*)}$ branching fractions, are given in the last row. Branching ratios for the D^0, D^{*+} and D^+ decays are taken from [5]. Table 4 gives the corresponding efficiencies for the topological analysis.

4 Narrow–Resonance Analysis

The production of narrow D^{**} states in the $D\ell\pi_{**}$ samples is tagged via $D^0\pi_{**}^+$ for charged D^{**} states and via $D^{*+}\pi_{**}^-$ and $D^+\pi_{**}^-$ for neutral D^{**} states. In the following, the parameter Δm^{**} is defined as the difference between the measured masses of the $D^{(*)}\pi_{**}$ system and the $D^{(*)}$. The resolution on this quantity is about 4 MeV/c^2, which is less than the natural widths of the D_1 and D_2^* resonances (cf. Table 1). For the various samples, the Δm^{**} distribution is examined for resonant structures. The Δm^{**} distributions obtained from data are shown in Fig. 4. For each sample, a right-sign and a wrong-sign distribution are shown. The wrong-sign samples are obtained by requiring the π_{**} to have the opposite

Channel	Signal Efficiency		
	$D^0 \pi_{**}^+ \ell^-$ (%)	$D^{*+} \pi_{**}^- \ell^-$ (%)	$D^+ \pi_{**}^- \ell^-$ (%)
$D^0 \to K^- \pi^+$	7.60±0.23	8.53±0.46	
$D^0 \to K^- \pi^+ \pi^- \pi^+$	2.44±0.12	5.67±0.38	
$D^0 \to K_S^0 \pi^+ \pi^-$	1.52±0.12	1.45±0.22	
$D^0 \to K^- \pi^+ \pi^0$	0.53±0.07	1.57±0.21	
$D^+ \to K^- \pi^+ \pi^+$			3.10±0.20
Overall Efficiency	0.60±0.02	1.04±0.06	0.28±0.03

Table 3: Efficiencies for the narrow–resonance $\overline{B} \to D^{**} \ell^- \overline{\nu}$ analysis. The last row reports the overall efficiencies, including D^0 and D^+ branching fractions, for the various samples. The uncertainties are due to Monte Carlo statistics.

Channel	Signal Efficiency		
	$D^0 \pi_{**}^+ \ell^-$ (%)	$D^{*+} \pi_{**}^- \ell^-$ (%)	$D^+ \pi_{**}^- \ell^-$ (%)
$D^0 \to K^- \pi^+$	5.00±0.19	4.77±0.27	
$D^0 \to K^- \pi^+ \pi^- \pi^+$	1.76±0.11	3.19±0.22	
$D^0 \to K_S^0 \pi^+ \pi^-$	1.13±0.10	0.70±0.10	
$D^0 \to K^- \pi^+ \pi^0$	0.41±0.07	0.76±0.12	
$D^+ \to K^- \pi^+ \pi^+$			2.35±0.20
Overall Efficiency	0.42±0.02	0.57±0.03	0.21±0.02

Table 4: Efficiencies for the topological analysis. The last row reports the overall efficiencies, including D^0 and D^+ branching fractions, for the various samples. The uncertainties are due to Monte Carlo statistics.

charge from that expected for D^{**} decay. An unbinned likelihood fit is performed on the right-sign Δm^{**} distributions; the fitted function is the sum of two or three Breit-Wigner functions, depending on the sample, convolved with a Gaussian resolution function, plus a background function of the form $\sqrt{\Delta m^{**} - m_\pi} \exp\left[-\beta(\Delta m^{**} - m_\pi)\right]$. The functions resulting from the unbinned fits are superimposed on the histograms of the right-sign distributions in Fig. 4.

4.1 Results

Results for $D^0 \pi_{**}^+$: For the $D^0 \pi_{**}^+$ sample, the right-sign Δm^{**} distribution is fitted to a background function and three Breit-Wigner functions convolved with Gaussian resolution functions. Two Breit-Wigner functions represent the production of $D_2^*(2460)^+$ decaying either directly to $D^0 \pi_{**}^+$ (*signal* peak) or via $D^{*0} \pi_{**}^+$ with $D^{*0} \to D^0 \pi^0/\gamma$ (*satellite* peak). The third Breit-Wigner function accounts for the $D_1(2420)^+$ decay via $D^{*0} \pi_{**}^+$. Since the neutral particle from the D^{*0} decay is not reconstructed, the latter two distributions appear shifted (and slightly broader). Two constraints are imposed in the fit. The mean of $D_2^*(2460)^+$ satellite peak has to be displaced from the $D_2^*(2460)^+$ signal peak by the amount expected due to the unmeasured particle. In addition, the amplitude of the $D_2^*(2460)^+$ satellite peak is constrained by the amplitude of the $D_2^*(2460)^+$ signal peak
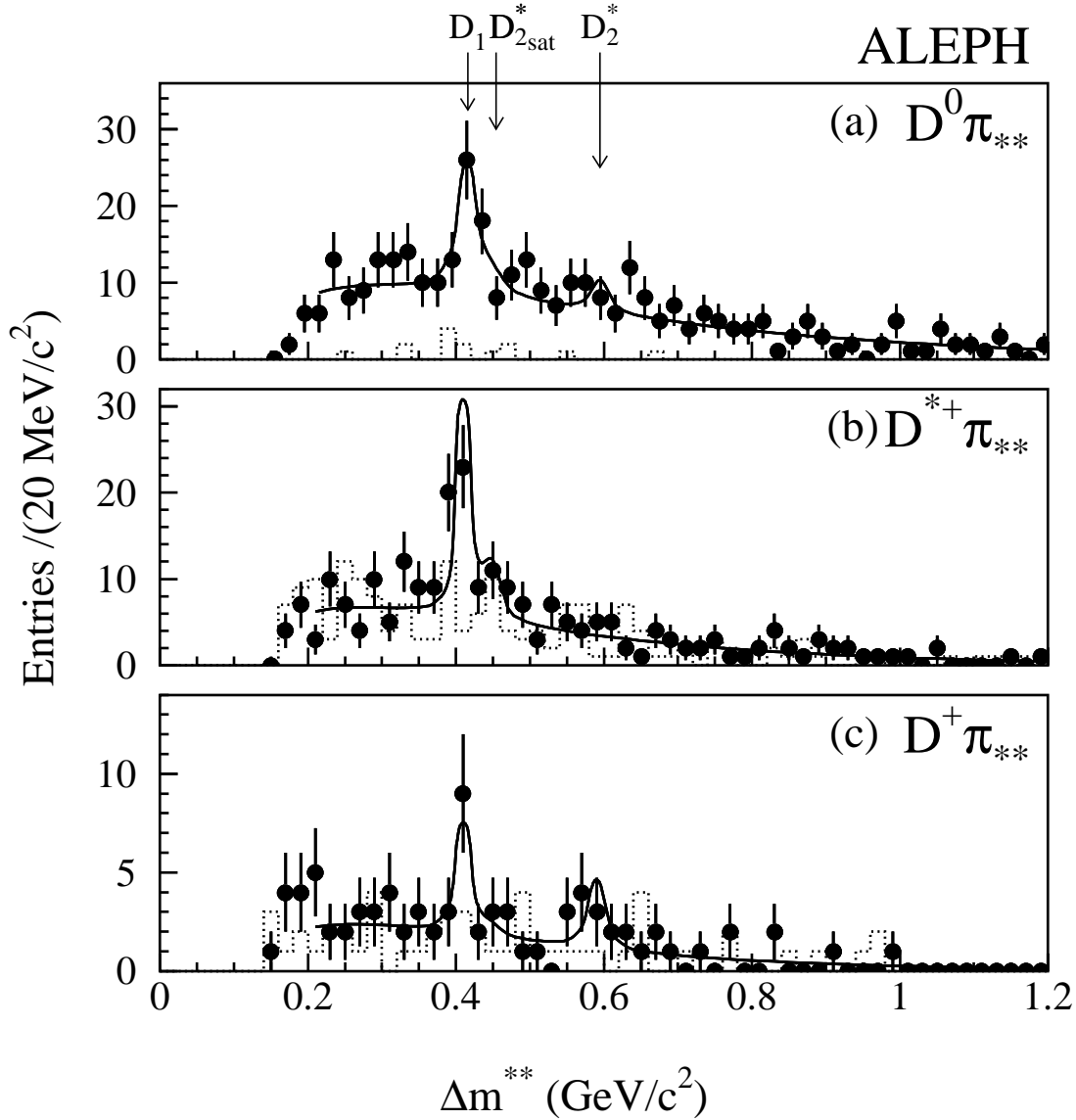
Figure 4: Δm^{**} distributions in the narrow–resonance analysis for the $D^0\pi_{**}$ (a), $D^{*+}\pi_{**}$ (b) and $D^+\pi_{**}$ (c) samples. Points and dashed lines represent the right-sign and wrong-sign $D^{(*)}\pi$ combinations, respectively. The superimposed lines result from the fits to the distributions with masses and widths of the D^{**} states fixed to their world average. The arrows indicate the position of the D_1 peak, and the D_2^* signal and satellite peaks.

according to the previously measured ratio [17]:

$$\frac{\mathrm{Br}(\mathrm{D}_2^* \longrightarrow \mathrm{D}\pi)}{\mathrm{Br}(\mathrm{D}_2^* \longrightarrow \mathrm{D}^*\pi)} = 2.3 \pm 0.8. \tag{1}$$

When the means and widths of the Breit-Wigner functions are fixed to world average values [5] in the fit, there are $40.2^{+10.8}_{-10.0}$ events in the $\mathrm{D}_1(2420)^+$ peak. From this number of events and the reconstruction efficiency, the following product branching ratio is obtained:

$$\mathrm{Br}(b \to \overline{\mathrm{B}}) \times \mathrm{Br}(\overline{\mathrm{B}} \to \mathrm{D}_1^+ \ell^- \overline{\nu} X) \times \mathrm{Br}(\mathrm{D}_1^+ \to \mathrm{D}^{*0}\pi^+) = (2.06^{+0.55}_{-0.51}(\mathrm{stat})^{+0.29}_{-0.40}(\mathrm{syst})) \times 10^{-3}.$$

The evaluation of systematic uncertainties is discussed in Section 4.2.

In the two $\mathrm{D}_2^*(2460)^+$ peaks, $8.8^{+6.9}_{-6.1}$ events are found. Using eqn. 1, the number of events under the signal peak is $6.1^{+4.8}_{-4.1}$. An upper limit on the production of the $\mathrm{D}_2^*(2460)^+$ can be set in the following way. Two windows of ± 2 half-widths around the $\mathrm{D}_2^*(2460)^+$ peaks are defined. The right-sign Δm^{**} distribution is refitted excluding events within the windows and dropping the terms for the $\mathrm{D}_2^*(2460)^+$ resonance. The integral of the resulting curve under the signal peak defines the background level, which consists of 15.8 events. In the data, 20 events are found. Using Poisson statistics, the $\mathrm{D}_2^*(2460)^+$ signal is thus 13.6 events or less at the 95% confidence level. Since only 70.5% of the area of a Breit-Wigner function is inside the window, the previous number must be rescaled. The upper limit on the product branching ratio at 95% confidence level is

$$\mathrm{Br}(b \to \overline{\mathrm{B}}) \times \mathrm{Br}(\overline{\mathrm{B}} \to \mathrm{D}_2^{*+} \ell^- \overline{\nu} X) \times \mathrm{Br}(\mathrm{D}_2^{*+} \to \mathrm{D}^0\pi^+) < 1.00 \times 10^{-3}.$$

When the fit is performed allowing the means of the Breit-Wigner functions to vary freely, there are $11.3^{+7.4}_{-6.5}$ $\mathrm{D}_2^*(2460)^+$ events and $38.7^{+11.0}_{-10.1}$ $\mathrm{D}_1(2420)^+$ events [2] . The fitted mass for the $\mathrm{D}_1(2420)^+$ peak is $2428.3^{+5.7}_{-5.6}\,\mathrm{MeV}/c^2$ which agrees with the world average of $2427 \pm 5\,\mathrm{MeV}/c^2$.

Results for $\mathrm{D}^{*+}\pi_{**}^-$: For the $\mathrm{D}^{*+}\pi_{**}^-$ sample the right-sign Δm^{**} distribution is fitted to a background function and two Breit-Wigner functions convolved with a Gaussian resolution function. The two Breit-Wigner functions represent respectively the decays of $\mathrm{D}_1(2420)^0$ and $\mathrm{D}_2^*(2460)^0$ via $\mathrm{D}^{*+}\pi_{**}^-$.

When the fit is performed fixing the means and widths of the two Breit-Wigner functions to the world average values [5], there are $38.8^{+9.3}_{-8.4}$ events in the $\mathrm{D}_1(2420)^0$ peak and $11.7^{+7.0}_{-6.1}$ events in the $\mathrm{D}_2^*(2460)^0$ peak. A product branching ratio for the production of $\mathrm{D}_1(2420)^0$ is obtained:

$$\mathrm{Br}(b \to \overline{\mathrm{B}}) \times \mathrm{Br}(\overline{\mathrm{B}} \to \mathrm{D}_1^0 \ell^- \overline{\nu} X) \times \mathrm{Br}(\mathrm{D}_1^0 \to \mathrm{D}^{*+}\pi^-) = (1.68^{+0.40}_{-0.36}(\mathrm{stat})^{+0.28}_{-0.29}(\mathrm{syst})) \times 10^{-3}.$$

Using the method discussed above, an upper limit product branching ratio for $\mathrm{D}_2^*(2460)^0$ production is obtained at 95% confidence level:

$$\mathrm{Br}(b \to \overline{\mathrm{B}}) \times \mathrm{Br}(\overline{\mathrm{B}} \to \mathrm{D}_2^{*0} \ell^- \overline{\nu} X) \times \mathrm{Br}(\mathrm{D}_2^{*0} \to \mathrm{D}^{*+}\pi^-) < 1.29 \times 10^{-3}.$$

---

[2] This procedure may result in a bias of the estimated number of events and is therefore not used in the calculation of the product branching ratios.

When the fit is performed allowing the mean of the $D_1(2420)^0$ Breit-Wigner function to vary freely, but keeping the $D_2^*(2460)^0$ mean fixed, there are $40.4^{+9.3}_{-8.4}$ events in the $D_1(2420)^0$ peak and $13.2^{+7.1}_{-6.2}$ events in the $D_2^*(2460)^0$ peak. The fitted mass for the $D_1(2420)^0$ peak is $2416.6 \pm 3.8\,\mathrm{MeV}/c^2$ which is consistent with the world average of $2422.0 \pm 2.1\,\mathrm{MeV}/c^2$.

Results for $\mathbf{D^+\pi^-_{**}}$: For the $D^+\pi^-_{**}$ sample the right-sign Δm^{**} distribution is fitted to a background function and three Breit-Wigner functions convolved with Gaussian resolution functions. The mass difference fit is identical to that used for the $D^0\pi^+_{**}$ sample.

When the means and widths of the Breit-Wigner functions are fixed to the world average values, there are $10.1^{+5.0}_{-4.1}$ events in the $D_1(2420)^0$ peak and $5.0^{+3.1}_{-2.6}$ events in the two $D_2^*(2460)^0$ peaks ($3.5^{+2.2}_{-1.8}$ in the signal peak, according to eqn. 1). A product branching ratio for the production of $D_1(2420)^0$ in this mode is obtained:

$$\mathrm{Br}(b \to \overline{B}) \times \mathrm{Br}(\overline{B} \to D_1^0 \ell^- \overline{\nu} X) \times \mathrm{Br}(D_1^0 \to D^{*+}\pi^-) = (3.62^{+1.78}_{-1.48}(\mathrm{stat}) \pm 0.77(\mathrm{syst})) \times 10^{-3}.$$

The 95% confidence level upper limit for product branching ratio for $D_2^*(2460)^0$ production is

$$\mathrm{Br}(b \to \overline{B}) \times \mathrm{Br}(\overline{B} \to D_2^{*0} \ell^- \overline{\nu} X) \times \mathrm{Br}(D_2^{*0} \to D^+\pi^-) < 1.26 \times 10^{-3}.$$

When the means of the Breit-Wigner functions are allowed to vary freely in the fit, there are $10.3^{+5.0}_{-4.1}$ events in the $D_1(2420)^0$ peak and $7.4^{+4.4}_{-3.5}$ events in the $D_2^*(2460)^0$ peaks. The fitted mass for the $D_1(2420)^0$ peak is to $2423.0\pm5.0\,\mathrm{MeV}/c^2$ which is consistent with the world average of $2422.0\pm2.1\,\mathrm{MeV}/c^2$.

4.2   Systematic Uncertainties

The systematic uncertainty due to the limited knowledge of the D^{**} masses and widths is computed by refitting the Δm^{**} distribution, varying the masses and widths of the resonances within their published values [5]. For the $D^0\pi^+_{**}$ and $D^+\pi^-_{**}$ fits, the uncertainty due to the error on the fixed ratio of the amplitudes of the D_2^* signal and satellite peaks is computed by refitting the Δm^{**} distribution and varying this quantity within its error.

In order to estimate the uncertainty due to the knowledge of the background shape, several different parameterizations are used to model the background in the fitting procedure. All of them are of the general form $(\Delta m^{**} - m_\pi)^\gamma \exp\left[-\beta((\Delta m^{**} - m_\pi)\right]$. In the analysis, the Δm^{**} distribution is fitted using $\gamma=0.5$. The distribution is refit setting $\gamma=0$ (purely exponential background shape) and it is also refit allowing γ to float freely, giving a background shape with an additional degree of freedom. The maximum deviation in the number of events observed in the signal peaks is taken as the systematic error.

The χ^2 probability requirement on the B and D vertices has been studied in inclusive $D^{(*)}\ell^-$ and $D^{(*)}$ events. The efficiency is well described by the Monte Carlo simulation and the systematic uncertainty is taken from the statistical precision of the comparison.

The lepton identification efficiency has been studied elsewhere and has an overall uncertainty of less than 2% [15].

The momentum distribution of the B hadrons is simulated with a fragmentation model which has been tuned to describe the observed distributions. The uncertainty

Source	Systematic uncertainty (10^{-3})		
	$D^0\pi^+_{**}\ell^-$	$D^{*+}\pi^-_{**}\ell^-$	$D^+\pi^-_{**}\ell^-$
Δm^{**} Fit Parameters	$^{+0.13}_{-0.29}$	$^{+0.17}_{-0.19}$	± 0.21
Background Function	± 0.19	± 0.16	± 0.61
Probability Function $\mathcal{P}$	± 0.07	± 0.05	± 0.12
Vertex Efficiency	± 0.06	± 0.05	± 0.18
Monte Carlo Statistics	± 0.06	± 0.07	± 0.23
D^{*+}, D^0, D^+ Branching Ratios	± 0.11	± 0.09	± 0.26
Lepton ID Efficiency	± 0.04	± 0.03	± 0.07
b Fragmentation	± 0.04	± 0.03	± 0.07
$\Gamma(Z\to b\bar{b})/\Gamma(Z\to\text{had})$	± 0.02	± 0.02	± 0.03
dE/dx	± 0.02	± 0.02	± 0.02
B Meson Lifetime	± 0.01	± 0.01	± 0.01
Total	$^{+0.29}_{-0.40}$	$^{+0.28}_{-0.29}$	± 0.77

Table 5: Systematic uncertainties on the triple product branching ratios for $D^0\pi^+_{**}\ell^-$, $D^{*+}\pi^-_{**}\ell^-$ and $D^+\pi^-_{**}\ell^-$ for the narrow–resonance analysis.

is estimated by varying the measured parameters describing the fragmentation spectrum in the simulation by their uncertainties [18] and observing the effect on the reconstruction efficiency.

Systematic uncertainties from the dE/dx measurements arise due to the availability of dE/dx information and the measured ionization for a given track. Detailed studies show that the overall effect on the selection efficiency is less than 0.4% and is dominated by the differences in the simulation of the ionization curves.

The systematic error associated with the B meson lifetime has been calculated by varying the lifetime within its published uncertainty [5]. The effect on the selection efficiency is negligible. An uncertainty due to the shape of the distribution of the impact parameter of the π_{**} with respect to the $D^{(*)}\ell^-$ vertex is calculated by varying the parameters of the fit to this distribution by their uncertainties.

Systematic uncertainties for the product branching ratios obtained from the $D^0\pi^+_{**}\ell^-$, $D^{*+}\pi^-_{**}\ell^-$ and $D^+\pi^-_{**}\ell^-$ samples are presented in Table 5. The dominant contributions are from the fit parameters and background function parameterization.

5   Topological Analysis

Signal processes for this study include those for the production of narrow D^{**} states discussed in Section 3 as well as the production of wide D^{**} and non-resonant $\overline{B}\to D^{(*)}\pi\ell^-\overline{\nu}$ decays. All processes have topologies similar to that illustrated in Fig. 1. Selection of these signal processes is accomplished using purely topological criteria, as described in Section 3. Since no attempt is made to distinguish between resonant and non-resonant decays, they are denoted generically as $\overline{B}\to D^{(*)}\pi\ell^-\overline{\nu}$.

The probability variable $\mathcal{P}$ described in Section 3.2 is used to estimate the number of signal events. Candidate π_{**} are required to have $\mathcal{P} > 0.2$. The contribution to the $\mathcal{P}$ distribution from combinatorial background is taken from $D^{(*)}\ell^-$ combinations which

have an invariant mass in the sidebands of the D mass distribution for the $D^0\pi^+_{**}$ and the $D^+\pi^-_{**}$ samples. The sidebands of the $D^{*+}-D^0$ mass difference distribution are used for the $D^{*+}\pi^-_{**}$ sample. The corresponding number of events with $\mathcal{P} > 0.2$ is subtracted after proper normalization. The contribution from fragmentation background to the $\mathcal{P}$ distribution is taken from the fraction of fragmentation pions that fall in the signal region, $\mathcal{P} > 0.2$, as estimated from simulated events.

However, since it is not possible to use the discriminating power of the resonant structures in invariant mass distributions, it is necessary to subtract specific *physics background* processes which may mimic the topology of signal events. The first of these processes results from the semileptonic decay of B_s^0 or Λ_b^0:

$$\overline{B}_s^0 \longrightarrow D_s^{**+}\ell^-\overline{\nu}X$$
$$\hookrightarrow D^{(*)0}K^+,$$

$$\overline{B}_s^0 \longrightarrow D^{(*)0}K^+\ell^-\overline{\nu}X,$$

$$\Lambda_b^0 \longrightarrow D^{(*)0}p\ell^-\nu X,$$

where the K^+ or p is mistakenly selected as a π_{**} candidate. These backgrounds have identical topologies to signal processes but affect only the measurement for $D^{(*)0}\pi^+$ final states. Particle identification on the π_{**} candidates is used to separate the $D^{(*)0}\pi^+$ sample from the others, as will be shown in Section 5.1. A branching ratio for $\overline{B} \to D^{(*)0}\pi^+\ell^-\overline{\nu}$ is extracted.

The other class of physics background comes from $b\to c\overline{c}s$ transitions resulting in hadronic final states with charm mesons that may decay semileptonically.

$$\overline{B} \longrightarrow D^{(*)} D_s^{(*)-}X$$
$$\hookrightarrow X'\ell\nu,$$
$$\overline{B} \longrightarrow D^{(*)}K^-\overline{D}^{(*)}X$$
$$\hookrightarrow X'\ell\nu,$$

where the K^- or a charged track due to X or X' is selected as a π_{**} candidate.

However, the leptons have a softer momentum spectrum than those of signal events. These backgrounds are suppressed by the cuts on lepton momentum and on the invariant mass of the $D^{(*)}\ell^-$ system. Monte Carlo simulations of $B\to D^{(*)}D_s^{(*)}$ decays have been used in order to evaluate the residual contamination. Assuming branching ratios as in [5], the number of events that fall in the $\mathcal{P} > 0.2$ signal region are 3.7 ± 1.9 for $D^0\pi^+$, 1.7 ± 0.9 for $D^{*+}\pi^-$, and 1.9 ± 1.0 for $D^+\pi^-$. Recent theoretical studies [19] predict that the branching ratio for decays of the type $Br(B\to D\overline{D}\,\overline{K}X)$ may be as large as $\sim 20\%$. The contribution of this process has been studied in a Monte Carlo simulation and is found to be negligible.

5.1 Results

Results for $D^0\pi^+_{**}$: When particle identification for the π^+_{**} candidate is required, it is possible to obtain a pion-enriched sample and a kaon-enriched sample. For the pion-enriched sample, the sum $R_K + R_\pi$ (see Section 2) is required to be greater than zero. For the kaon-enriched sample, this cut is reversed. Tracks without ionization measurements are assigned to the pion–enriched sample.
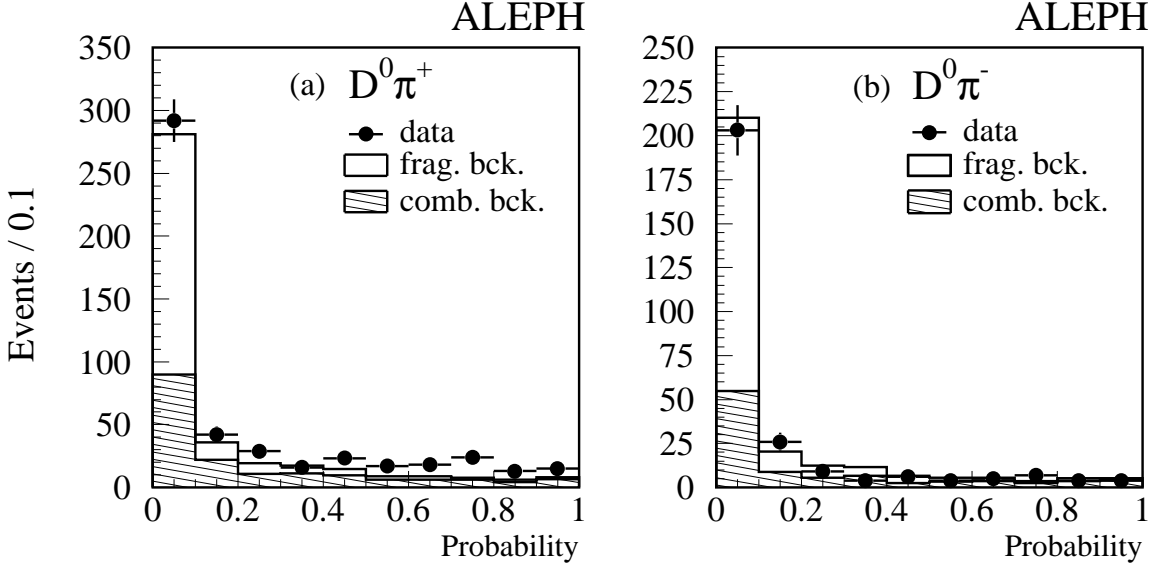
Figure 5: Probability distribution (points) for the pion-enriched sample for the right-sign sample (a) and the wrong-sign sample (b). Contributions from fragmentation and combinatorial background are also shown.
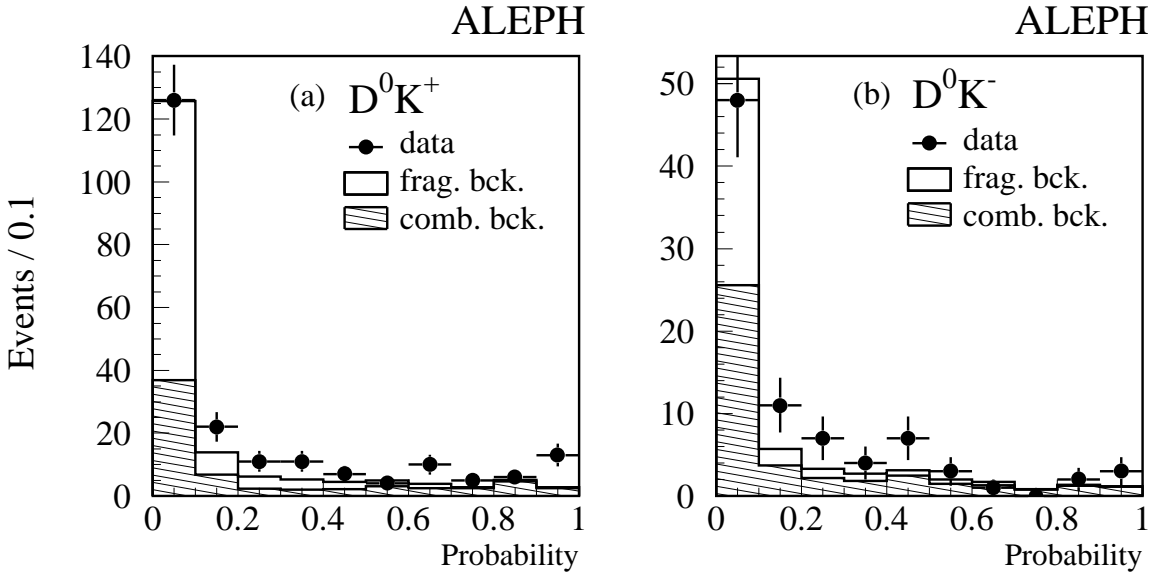

Figure 6: Probability distribution for the kaon-enriched sample for the right-sign sample (a) and the wrong-sign sample (b). Contributions from fragmentation and combinatorial backgrounds are also shown.

14

The overall B and B_s^0 signal process efficiencies are respectively $(0.32\pm0.02)\%$ and $(0.12\pm0.01)\%$ for the pion–enriched sample, $(0.061\pm0.005)\%$ and $(0.27\pm0.02)\%$ for the kaon–enriched sample[3] .

Figures 5 and 6 show the right-sign and wrong-sign probability distributions for the pion-enriched and kaon-enriched samples. A clear excess over the background is seen in the right-sign combination; no significant excess is present in the wrong-sign combination. The invariant mass distribution for the pion-enriched sample is shown in Fig. 9a, for right-sign and wrong-sign combinations. The number of signal events in the $\mathcal{P} > 0.2$ region after background subtraction is respectively $65.9 \pm 14.3 \pm 9.0$ for the pion-enriched sample and $30.7\pm9.5\pm5.4$ for the kaon-enriched sample. Combining the two results, it is possible to isolate the genuine contribution from signal decays, leading to the result:

$$\mathrm{Br}(b \to \overline{\mathrm{B}}) \times [\mathrm{Br}(\overline{\mathrm{B}} \to \mathrm{D}^0\pi^+\ell^-\overline{\nu}X) + \mathrm{Br}(\overline{\mathrm{B}} \to \mathrm{D}^{*0}\pi^+\ell^-\overline{\nu}X)]$$
$$= (4.65 \pm 1.33(\mathrm{stat}) \pm 1.00(\mathrm{syst})) \times 10^{-3}.$$

The corresponding sum of the decay rates for processes involving kaons and protons (presumably B_s^0 and Λ_b^0) is $(2.58\pm1.19\pm0.79)\times10^{-3}$.

Results for $\mathrm{D}^{*+}\pi_{**}^-$: The probability distributions and invariant mass distributions for right-sign and wrong-sign samples for $\mathrm{D}^{*+}\pi_{**}^-$ are shown in Fig. 7 and 9b.
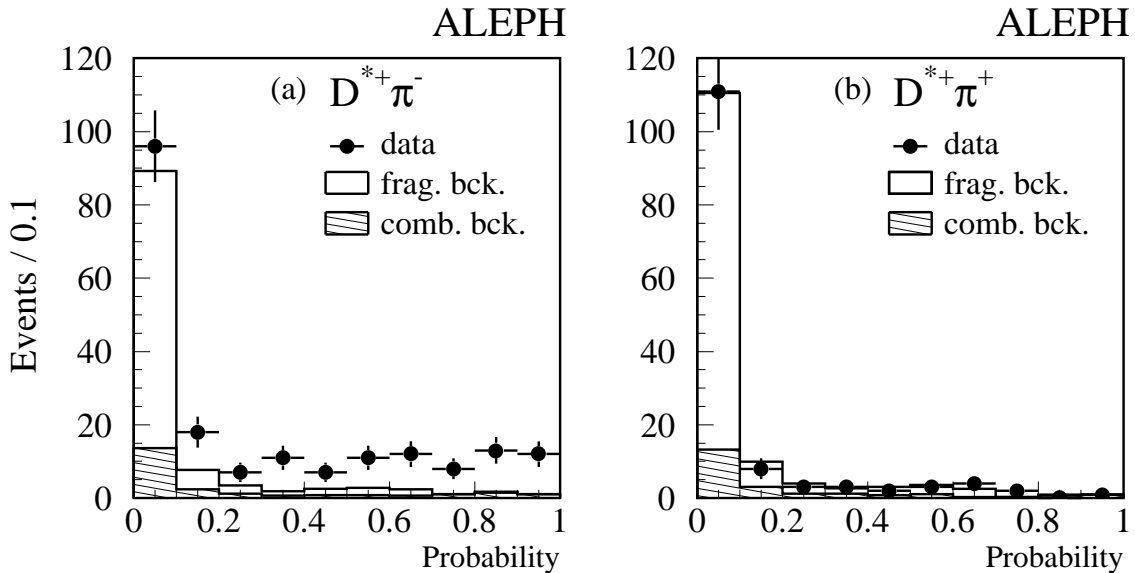

Figure 7: Probability distribution for the right-sign sample (a) and the wrong-sign sample (b) for the $\mathrm{D}^{*+}\pi^-$ topological analysis. Contributions from fragmentation and combinatorial backgrounds are also shown.

The number of signal events in the $\mathcal{P} > 0.2$ region after background subtraction is

---

[3] The kaon–enriched sample is assumed to include a contribution from protons (*i.e.*, from Λ_b^0 decays). The relative contribution of Λ_b^0 with respect to B_s^0 decays is estimated to be $(17\pm5)\%$, from Monte Carlo simulations.
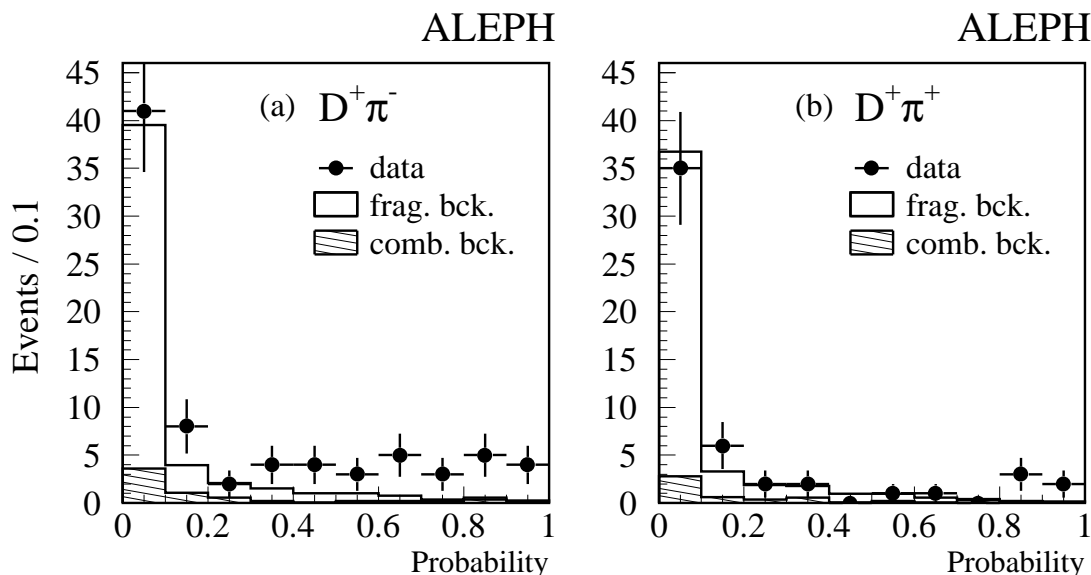
Figure 8: Probability distribution for the right-sign sample (a) and the wrong-sign sample (b) for the $D^+\pi^-$ topological analysis. Contributions from fragmentation and combinatorial backgrounds are also shown.

$59.2 \pm 9.6 \pm 2.6$. For comparison, the corresponding number of events in the wrong-sign sample is $-1.3 \pm 5.1 \pm 2.4$. The branching ratio for the sum of the resonant D^{**} and non-resonant contributions is

$$\mathrm{Br}(b \to \overline{B}) \times \mathrm{Br}(\overline{B} \to D^{*+}\pi^-\ell^-\overline{\nu}\, X) = (4.73 \pm 0.77(\mathrm{stat}) \pm 0.55(\mathrm{syst})) \times 10^{-3}.$$

Results for $D^+\pi^-_{**}$: The probability distributions and invariant mass distributions for right-sign and wrong-sign samples for $D^+\pi^-_{**}$ are shown in Fig. 8 and 9c. The number of signal events in the $\mathcal{P} > 0.2$ region after background subtraction is $20.5 \pm 5.1 \pm 1.4$. The corresponding number of events in the wrong-sign sample is $4.0 \pm 3.5 \pm 1.3$. The branching ratio for the sum of the resonant D^{**} and non-resonant contributions is

$$\mathrm{Br}(b \to \overline{B}) \times [\mathrm{Br}(\overline{B} \to D^+\pi^-\ell^-\overline{\nu}X) + \mathrm{Br}(\overline{B} \to D^{*+}\pi^-\ell^-\overline{\nu}X) \times \mathrm{Br}(D^{*+} \to D^+\pi^0/\gamma)]$$
$$= (2.98 \pm 0.74(\mathrm{stat})^{+0.56}_{-0.52}(\mathrm{syst})) \times 10^{-3}.$$

5.2   Systematic Uncertainties

Systematic uncertainties for the topological analysis are similar to those discussed in Section 4.2. An additional uncertainty arises from the unknown fraction of narrow, wide, and non-resonant decays, which affects the momentum spectrum of the π_{**}. The π_{**} momentum spectra for the wide and non-resonant cases are similar and are considerably harder than for the narrow–resonance case. An estimate of this effect is obtained by varying the fraction of narrow–resonance decays in the simulation from 0 to 100%. The maximum difference on the reconstruction efficiency is 10%, which is taken conservatively
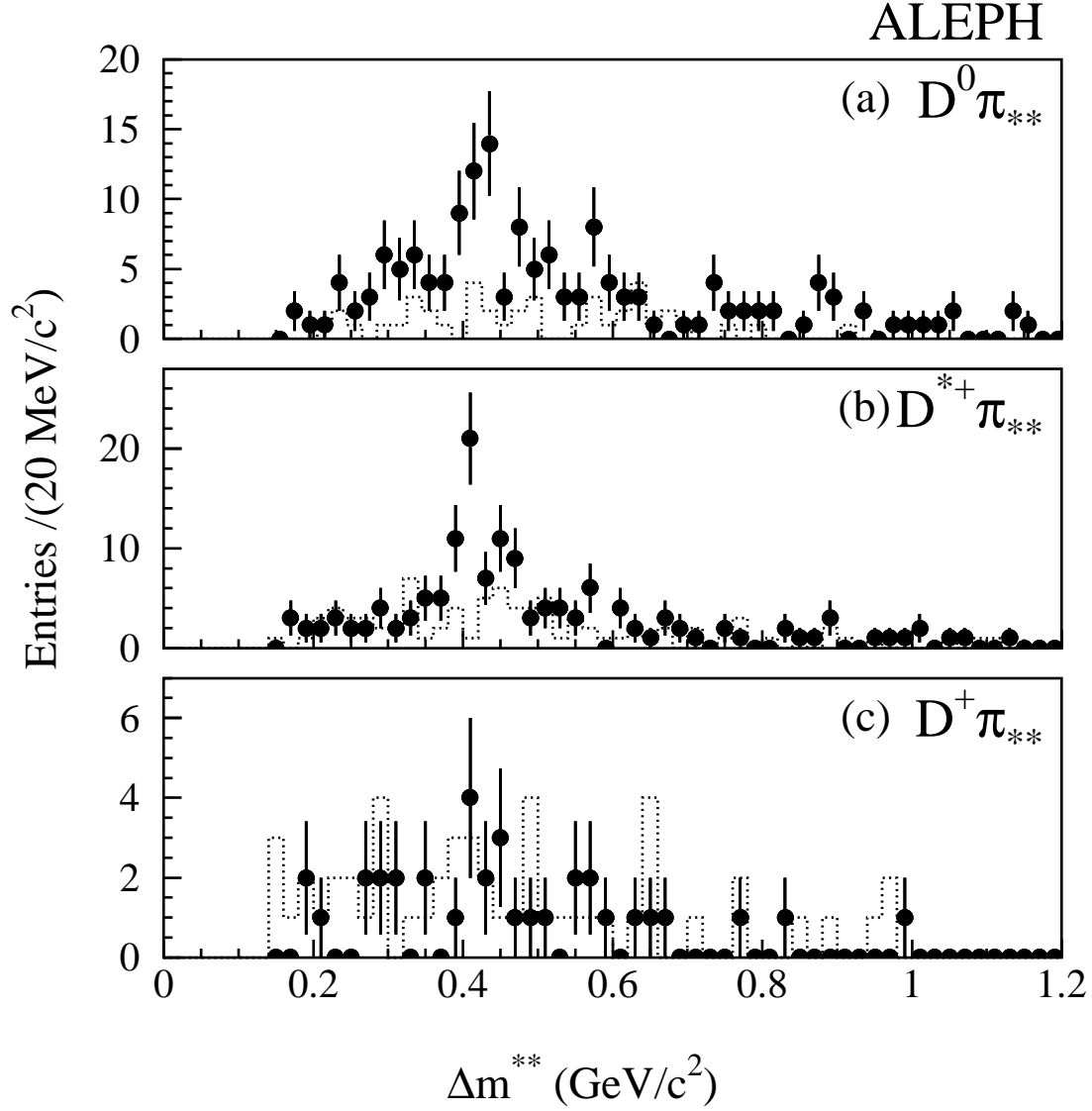
Figure 9: The Δm_{**} distributions for the topological analysis for the $\mathrm{D}^0\pi_{**}$ (a), $\mathrm{D}^{*+}\pi_{**}$ (b), and $\mathrm{D}^+\pi_{**}$ (c) samples. Points and dashed lines represent the right-sign and wrong-sign $\mathrm{D}^{(*)}\pi$ combinations, respectively.

as the systematic uncertainty. The error due to the background subtraction procedure is also included. The systematic uncertainties for the product branching ratios for the various samples are given in Table 6.

Source	Systematic uncertainty (10^{-3})		
	$D^0\pi_{**}^+\ell^-$	$D^{*+}\pi_{**}^-\ell^-$	$D^+\pi_{**}^-\ell^-$
Wide vs. non.res. effic.	$^{+0.29}_{-0.32}$	$^{+0.27}_{-0.29}$	$^{+0.33}_{-0.27}$
Background Subtraction	±0.83	±0.24	±0.20
Probability Function $\mathcal{P}$	±0.16	±0.15	±0.10
Monte Carlo Statistics	±0.23	±0.22	±0.28
Vertex Efficiency	±0.15	±0.14	±0.15
Lepton ID Efficiency	±0.09	±0.09	±0.06
$D^{(*)}$ Branching Ratios	±0.31	±0.26	±0.20
b Fragmentation	±0.06	±0.09	±0.06
$\Gamma(Z\to b\overline{b})/\Gamma(Z\to had)$	±0.04	±0.04	±0.03
dE/dx	±0.02	±0.02	±0.02
B Meson Lifetime	±0.01	±0.01	±0.01
Total	±1.00	±0.55	$^{+0.56}_{-0.52}$

Table 6: Systematic uncertainties on product branching ratios in the topological analysis for $D^0\pi_{**}^+\ell^-$, $D^{*+}\pi_{**}^-\ell^-$ and $D^+\pi_{**}^-\ell^-$ samples.

6 Summary and Interpretation of Results

Table 7 summarizes the measurements of the semileptonic B branching ratios presented in the previous sections.

The two measurements of the branching ratio for the D_1^0 from the $D^{*+}\pi^-$ and $D^+\pi^-$ samples can be combined to yield

$$\text{Br}(b \to \overline{B}) \times \text{Br}(\overline{B} \to D_1^0\ell^-\overline{\nu}X) \times \text{Br}(D_1^0 \to D^{*+}\pi^-) = (1.78^{+0.39}_{-0.35}(\text{stat})^{+0.27}_{-0.29}(\text{syst})) \times 10^{-3}.$$

Using isospin invariance, the measurement for the D_1^+ may be averaged with the above measurements yielding

$$\text{Br}(b \to \overline{B}) \times \text{Br}(\overline{B} \to D_1\ell^-\overline{\nu}X) \times \text{Br}(D_1 \to D^*\pi) = (1.87^{+0.32}_{-0.29}(\text{stat})^{+0.23}_{-0.25}(\text{syst})) \times 10^{-3}.$$

Assuming that the D_1 decays into $D^*\pi$ only, isospin symmetry gives $\text{Br}(D_1 \to D^*\pi^\pm)=2/3$. Using the value $\text{Br}(b \to \overline{B})=(37.8\pm2.2)\%$ [5] and assuming that no other particle is produced in the B decay yields

$$\text{Br}(\overline{B} \to D_1\ell^-\overline{\nu}) = (0.74 \pm 0.16)\%. \tag{2}$$

Under the same assumptions as above, upper limits in the range 1.5–2.0 $\times10^{-3}$ are set for the $\overline{B} \to D_2^*\ell^-\overline{\nu}$ branching ratios.

The sum of decays giving a $D^+\pi^-$ or a $D^{*+}\pi^-$ is

$$\text{Br}(b \to \overline{B}) \times \left[\text{Br}(\overline{B} \to D^+\pi^-\ell^-\overline{\nu}X) + \text{Br}(\overline{B} \to D^{*+}\pi^-\ell^-\overline{\nu}X)\right]$$
$$= (6.20 \pm 0.91(\text{stat})^{+0.85}_{-0.81}(\text{syst})) \times 10^{-3},$$

Product Branching Ratio $\text{Br}(b \to \overline{\text{B}}) \times$	(10^{-3})
Narrow–resonance analysis	
$\text{Br}(\overline{\text{B}} \to \text{D}_1^+ \ell^- \overline{\nu} X) \times \text{Br}(\text{D}_1^+ \to \text{D}^{*0}\pi^+)$	$2.06^{+0.55+0.29}_{-0.51-0.40}$
$\text{Br}(\overline{\text{B}} \to \text{D}_1^0 \ell^- \overline{\nu} X) \times \text{Br}(\text{D}_1^0 \to \text{D}^{*+}\pi^-)$	$1.68^{+0.40+0.28}_{-0.36-0.29}$
$\text{Br}(\overline{\text{B}} \to \text{D}_1^0 \ell^- \overline{\nu} X) \times \text{Br}(\text{D}_1^0 \to \text{D}^{*+}\pi^-)$ (via $\text{D}^+\pi^-\pi^0/\gamma$)	$3.62^{+1.78}_{-1.48} \pm 0.77$
$\text{Br}(\overline{\text{B}} \to \text{D}_2^{*+} \ell^- \overline{\nu} X) \times \text{Br}(\text{D}_2^{*+} \to \text{D}^0\pi^+)$	< 1.00 (95% C.L.)
$\text{Br}(\overline{\text{B}} \to \text{D}_2^{*0} \ell^- \overline{\nu} X) \times \text{Br}(\text{D}_2^{*0} \to \text{D}^{*+}\pi^-)$	< 1.29 (95% C.L.)
$\text{Br}(\overline{\text{B}} \to \text{D}_2^{*0} \ell^- \overline{\nu} X) \times \text{Br}(\text{D}_2^{*0} \to \text{D}^+\pi^-)$	< 1.26 (95% C.L.)
Topological analysis	
$\text{Br}(\overline{\text{B}} \to \text{D}^0\pi^+ \ell^- \overline{\nu} X) + \text{Br}(\overline{\text{B}} \to \text{D}^{*0}\pi^+ \ell^- \overline{\nu} X)$	$4.65 \pm 1.33 \pm 1.00$
$\text{Br}(\overline{\text{B}} \to \text{D}^{*+}\pi^- \ell^- \overline{\nu} X)$	$4.73 \pm 0.77 \pm 0.55$
$\text{Br}(\overline{\text{B}} \to \text{D}^+\pi^- \ell^- \overline{\nu} X)$ $+ \text{Br}(\overline{\text{B}} \to \text{D}^{*+}\pi^- \ell^- \overline{\nu} X) \times \text{Br}(\text{D}^{*+} \to \text{D}^+\pi^0/\gamma)$	$2.98 \pm 0.74^{+0.56}_{-0.52}$

Table 7: Summary of the semileptonic B branching ratios measured in this paper. The first quoted uncertainty is statistical, the second is systematic.

which is in agreement with its isospin conjugate

$$\text{Br}(b \to \overline{\text{B}}) \times \left[\text{Br}(\overline{\text{B}} \to \text{D}^0\pi^+\ell^-\overline{\nu}X) + \text{Br}(\overline{\text{B}} \to \text{D}^{*0}\pi^+\ell^-\overline{\nu}X) \right]$$
$$= (4.65 \pm 1.33(\text{stat}) \pm 1.00(\text{syst})) \times 10^{-3}.$$

If it is assumed that all $\text{D}^0\pi^+$, $\text{D}^{*0}\pi^+$, $\text{D}^+\pi^-$ and $\text{D}^{*+}\pi^-$ come from D^{**} resonances then combining the two above results and assuming isospin invariance yields

$$\text{Br}(b \to \overline{\text{B}}) \times \left[\text{Br}(\overline{\text{B}} \to \text{D}\pi\ell^-\overline{\nu}) + \text{Br}(\overline{\text{B}} \to \text{D}^*\pi\ell^-\overline{\nu}) \right]$$
$$= (8.55 \pm 1.13(\text{stat})^{+1.18}_{-1.14}(\text{syst})) \times 10^{-3},$$

which corresponds to

$$\text{Br}(\overline{\text{B}} \to \text{D}\pi\ell^-\overline{\nu}) + \text{Br}(\overline{\text{B}} \to \text{D}^*\pi\ell^-\overline{\nu}) = (2.26 \pm 0.29(\text{stat}) \pm 0.33(\text{syst}))\%. \qquad (3)$$

This branching ratio is $(20\pm5)\%$ of the inclusive rate and, together with the previously measured branching ratios for $\overline{\text{B}} \to \text{D}\ell^-\overline{\nu}$ and $\overline{\text{B}} \to \text{D}^*\ell^-\overline{\nu}$, sums to $(76\pm8)\%$ of the inclusive rate for semileptonic B decays. Table 8 presents a summary of the measured exclusive B semileptonic branching ratios and the corresponding fractions of the inclusive rate for which they account. The values for previously measured exclusive modes are taken from [5]. The inclusive rate is derived from [20], where a correction has been applied to account for the production of B_s^0 and Λ_b^0.

However, it should be noted that these results hold under specific assumptions. In particular, if the contribution of three-body, rho and eta decays of the D^{**} is sizeable [21], the branching ratio (2) should be taken as a lower limit and no conclusion can be drawn for the production of D_2^*. Furthermore, contamination of the $\text{D}^{(*)}\pi$ samples by these decays may contribute to the measured branching ratio (3).

Decay	Branching Ratio (%)		Fraction (%)
B→Dℓ⁻ν̄	1.8±0.4	[5]	16±4
B→D*ℓ⁻ν̄	4.6±0.3	[5]	40±4
Sum	6.4±0.5		56±6
B→D*πℓ⁻ν̄ +B→Dπℓ⁻ν̄	2.3±0.4	This measurement	20±5
Total	8.7±0.7		76±8
Inclusive rate	11.5±0.7	[20]	–

Table 8: Summary of the measured exclusive branching ratios for semileptonic B meson decay.

7 Conclusion

A measurement of the semileptonic decay rates of B mesons into $D^{(*)}\pi$ final states has been performed with the ALEPH detector at LEP. The method employed is sensitive to narrow and wide D^{**} states, as well as to non–resonant decays. Under specific assumptions, the semileptonic branching ratio of B mesons into the D_1 is measured to be

$$\mathrm{Br}(\overline{B} \to D_1 \ell^- \bar{\nu}) = (0.74 \pm 0.16)\%.$$

Upper limits at the 95% confidence level are set in the range 1.5–2.0 $\times 10^{-3}$ for the production of D_2^* mesons.

The branching ratio for the sum of all semileptonic decays containing a $D^{(*)}\pi$ in the final state is measured to be

$$\mathrm{Br}(\overline{B} \to D\pi\ell^-\bar{\nu}) + \mathrm{Br}(\overline{B} \to D^*\pi\ell^-\bar{\nu}) = (2.26 \pm 0.29(\mathrm{stat}) \pm 0.33(\mathrm{syst}))\%.$$

The decays into narrow D^{**} states explain (6±1)% of the inclusive rate; the sum of the semileptonic decays producing a $D^{(*)}\pi$ pair in the final state accounts for at least (20±5)% and, together with the decays into D and D*, for at least (76±8)% of the inclusive rate.

Acknowledgements

References

[1] M. Voloshin and M. Shifman, *Sov. J. Nucl. Phys.* **45** (1987) 292;
    M. Voloshin and M. Shifman, *Sov. J. Nucl. Phys.* **47** (1988) 511;
    N. Isgur, D. Scora, B. Grinstein, and M. B. Wise, *Phys. Rev.* **D39** (1989) 799;
    P. Colangelo, G. Nardulli and N. Paver, *Phys. Lett.* **B293** (1992) 207.

[2] M. Neubert, *Phys. Reports* **245** (1994) 259.

[3] H. Albrecht *et al.*(ARGUS Collaboration), *Phys. Lett.* **B221** (1989) 422;
    H. Albrecht *et al.*(ARGUS Collaboration), *Phys. Lett.* **B232** (1989) 398;
    J.C. Anjos *et al.*(E691 Collaboration), *Phys. Rev. Lett.* **62** (1989) 1717;
    P. Avery *et al.*(CLEO Collaboration), *Phys. Rev.* **D41** (1990) 774;
    P.L. Frabetti *et al.*(E687 Collaboration), *Phys. Rev. Lett.* **72** (1994) 324;
    P. Avery *et al.*(CLEO II Collaboration), *Phys. Lett.* **B331** (1994) 236.

[4] H. Albrecht *et al.*(ARGUS Collaboration), *Phys. Lett.* **B231** (1989) 208;
    P.L. Frabetti *et al.*(E687 Collaboration), *Phys. Rev. Lett.* **72** (1994) 324;
    T. Bergfeld *et al.*(CLEO II Collaboration) *Phys. Lett.* **B340** (1994) 194.

[5] L. Montanet *et al.*(Particle Data Group), *Phys. Rev.* **D50** (1994) 1173;
    the values of the masses and widths of the D^{**} states and $Br(b \to \overline{B})$ are taken from
    R.M. Barnett *et al.*(Particle Data Group), *Phys. Rev.* **D54** (1996) 1.

[6] S. Godfrey and N. Isgur, *Phys. Rev.* **D32** (1985) 189;
    S. Godfrey and R. Kokoski, *Phys. Rev.* **D43** (1991) 1679;
    A.B. Kaidalov and A.V. Nogteva, *Sov. J. Nucl. Phys.* **47** (1988) 321;
    J. Rosner, *Comments on Nuclear and Particle Physics* **16** (1986) 109.

[7] D. Buskulic *et al.*(ALEPH Collaboration), *Phys. Lett.* **B345** (1994) 103.

[8] H. Albrecht *et al.*(ARGUS Collaboration), *Z. Phys.* **C57** (1993) 533.

[9] R. Akers *et al.*(OPAL Collaboration), *Z. Phys.* **C67** (1995) 57.

[10] J.P. Alexander *et al.*(CLEO Collaboration), CLEO CONF 95-30, contributed paper
    to the XXVIII International Conference on High Energy Physics, Bruxelles, Belgium,
    1995, reference EPS0168.

[11] P. Abreu *et al.*(DELPHI Collaboration), CERN-PPE-96-11, submitted to *Z. Phys.*

[12] D. Decamp *et al.* (ALEPH Collaboration), *Nucl. Instr. Meth.* **A294** (1990) 121.

[13] D. Buskulic *et al.*(ALEPH Collaboration), *Nucl. Instr. Meth.* **A360** (1995) 481.

[14] G. Batignani *et al.*, IEEE Trans. Nuc. Sci. **39** (1992) 701.

[15] D. Buskulic *et al.*(ALEPH Collaboration), *Nucl. Instr. Meth.* **A436** (1994) 461.

[16] D. Buskulic *et al.*(ALEPH Collaboration), *Phys. Lett.* **B313** (1993) 535.

[17] P. Avery *et al.*(CLEO II Collaboration), *Phys. Lett.* **B331** (1994) 236;
H. Albrecht *et al.*(ARGUS Collaboration), *Phys. Lett.* **B232** (1989) 398.

[18] D. Buskulic *et al.*(ALEPH Collaboration), *Phys. Lett.* **B357** (1995) 699.

[19] G. Buchalla, I. Dunietz and H. Yamamoto, *Phys. Lett.* **B364** (1995) 188.

[20] The Four LEP Collaborations and the LEP Heavy-Flavour Electroweak Working Group, Preprint CERN–PPE/95–172.

[21] E.J. Eichten, C.T. Hill and C. Quigg, *Phys. Rev. Lett.* **71** (1993) 4116;
A.F. Falk and M. Luke, *Phys. Lett.* **B292** (1992) 119.